Surface Morphology of Blended Molding Pellets Made of Desert Caragana and Maize Stover

Xuehong De,[a] Bowen Zhang,[a] Wenbin Guo,[a,*] Jiawei Yang,[a] Jianchao Zhang,[a] and Xiaomin Zhai [b]

The surface morphology of biomass pellets can provide data for the contact mechanics fractal model between the molding pellet and hole in biomass molding machines and for predicting wear of the molding hole. In this study, desert caragana (*Caragana korshinskii*) was mixed with residue from maize production, crushed, and compressed into pellets, which were used to collect data on their circumferential surface roughness profile, density, diameter, and hardness. The results showed that frictional wear occurs during contact between the forming hole and the molding particles, increasing the diameter d_0 of the forming hole and the diameter d of the molding particles. The density ρ and hardness HD of the molded pellets decreased as their diameter d increased, and the ρ and HD of caragana were higher in autumn than in summer. The values of the roughness parameters R_a, R_c and R_z of the molded particles increased with their diameter d. The maximum material rate M_{r2} value of the roughness's central profile remained at 86% with the increase of diameter d. Molded particles had surface roughness kurtosis R_{ku}>3 and roughness skew R_{sk}<0 with the increase of diameter d. The surface of molded particles was spiky and negatively skewed, and with a low number of spikes.

DOI: 10.15376/biores.18.2.3019-3032

Keywords: Desert caragana; Molding pellets; Roughness parameters; Density; Morphological analysis

*Contact information: a: College of Mechanical and Electrical Engineering, Inner Mongolia Agricultural University, Hohhot 010020, PR China; b: Sixth Research Institute, China Aerospace Science & Industry Corp, Hohhot 010076, PR China; *Corresponding author:wenbingwb2000@sina.com*

INTRODUCTION

The particles molded by mixing desert caragana (*Caragana korshinskii*) and maize stover were made from caragana with a certain particle size and moisture content and different proportions of stover, which were compressed by a biomass ring molding machine under external force to make pellets with a certain diameter size and density (Jiang *et al*. 2020; Zhang *et al*. 2020a). In the process of being compressed, contact friction is generated between the forming particles and the ring die forming holes in contact with each other, and when the frictional heat reaches the lignin softening temperature of about 100 °C, the raw material is extruded into pellets (De *et al*. 2014). In this process, the forming particles cause some wear on the contact surface inside the forming die holes. When the amount of wear on the contact surfaces in the mold hole reaches a certain value, the ratio of the length to the diameter of the mold hole (Length to diameter ratio) h/d_0 decreases, affecting the quality of the molded particles. When h/d_0 drops to a certain limit, the forming die hole cannot compress out qualified forming particles and the forming machine is scrapped (Ning *et al*. 2016; Jiao 2020; Wang *et al*. 2021; Yu 2021). Research on the microstructure of the

circumferential surface of molding particles is the basis for the establishment of a contact fractal model between the molding holes and the circumferential surface of forming particles, the analysis of the contact friction wear mechanism, and the prediction of wear (Duan and Chen 2017; Nieslony *et al*. 2018; Liu *et al*. 2020b; Qiu *et al*. 2020; Mao 2021; Song *et al*. 2021; Zhang *et al*. 2021).

It is possible to analyze the surface profile morphology of the particles based on the following: the shape sharpness R_{ku} (roughness kurtosis) of the roughness profile height amplitude curve relative to the average line; and the asymmetric skew R_{sk} (roughness skew) of the profile height amplitude curve relative to the average line. R_{ku}>3 indicates it is a spiky surface with a high kurtosis value; R_{ku}=3 indicates it is an excellent arbitrary surface kurtosis value; R_{sk}<0 (high grinding surface) indicates it is an asymmetrical negative skewed surface with fewer profile spikes and a strong surface bearing capacity; R_{sk}=0 (geodesic surface); and R_s>0 (rotary surface) indicates it is an asymmetrical positive skewed surface with more profile spikes and a weaker surface bearing capacity, requiring grinding. This system can be used as an important basis for modeling the mechanics of the contact between the mold hole and the molded particles (An *et al*. 2020; Huang *et al*. 2020; Xiao *et al*. 2020; Shi *et al*. 2020; Zhang *et al*. 2020b).

For this study, molding particles were chosen for mixing caragana and stover in different proportions, which are compressed by a ring molding machine with a mold hole diameter of d_0 of 8 mm. Data were collected for their circumferential surface roughness profile, density, diameter, and hardness. Correlations among these quantities were analyzed. By analyzing the surface morphological characteristics, the pattern between the surface roughness parameters of the biomass molding pellets and the forming die holes of the key components of the ring die was explored. Such work provided base data for modeling the fractal contact between the forming pellet and the forming die hole, as well as for accurately analyzing the mechanical contact between the surface of the biomass molding pellets and the forming die (Falconer 1989; Huang 2020; Liu *et al*. 2020a; Schweinhart 2020; De *et al*. 2021).

Theoretical Analysis

The rough surface profile of the biomass forming pellet circumference is the basis for an accurate analysis of the interaction between the surface of the biomass forming pellet and the forming die. It is also the key to analyze the frictional wear mechanisms to which the forming die is subjected and to predict the wear. Fractal theory can be used to gain insight into the fine structure hidden in the chaotic natural phenomena within things. It is well suited to describing phenomena characterized by scalar rates, and the rough surface profile of the circumference of caragana strip-formed particles has statistical self-similarity and scale-invariance. The use of fractal theory to study the real contact between metal contact surfaces has been carried out and can also be used to explore the real contact between biomass forming particles and the inner wall of the forming hole (Falconer 1989; Huang *et al*. 2020; Liu *et al*. 2020).

Frictional Surface Contact Condition

It was assumed that the forming channel and the biomass pellet are element O1 and O2 of the friction pair, respectively, and the corresponding contour lines of the contacting surface S1 and S2 before contact deformation happens are $z_1(x)$ and $z_2(x)$, respectively. At the smallest scale, there is a point B_1 in contact with a certain micro-convex body pair *i* at a certain moment, and after a certain time and relative sliding distance *S*, the dashed line

indicates the profile when undeformed. Considering the elastic-plastic deformation, let A_i be the contact surface and let $\delta_1^{(i)}$ and $\delta_2^{(i)}$ be its deformations, respectively, projected in the horizontal x and vertical z directions $\delta_{x1}^{(i)}$, $\delta_{z1}^{(i)}$ and $\delta_{x2}^{(i)}$, $\delta_{z2}^{(i)}$, when due to deformation and relative sliding along the contact surface (Ge *et al*. 2005), the amount of change in the vertical distance between the two contact surfaces $\Delta h = Stan\beta - (\delta_{z1}^{(i)} + \delta_{z2}^{(i)}) = Stan\beta - \delta_{zi}$ (β is the inclination angle of the micro-contact surface, $tan\beta = \partial z1/\partial x1$, z_1 and x_1 are its projections in the z,x direction). For a certain relative sliding velocity V_x along the x-direction of the surface contact friction sub-element, its relative sliding velocity V_z in the z-direction depends on the surface morphological characteristics and mechanical properties, set $V_x = \partial S/\partial t$, $V_z = \partial h/\partial t$, the two sides of Δh to time t derivative has $V_z = \partial h/\partial t = V_x - \partial z1/\partial x1 - \partial \delta_z^{(i)}/\partial t$.

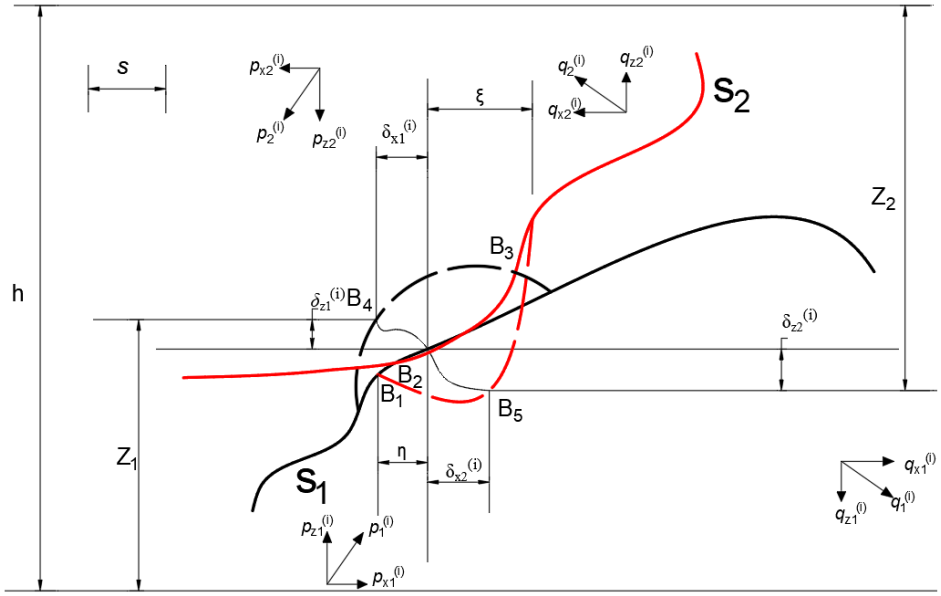

Fig. 1. Analysis of the contact state and forces of a pair of micro asperity after a relative sliding distance

Microscopic Contact Mechanics Analysis

In the contact region (Fig. 1), the microconvex body has a mechanical deformation resistance q and a molecular adhesion resistance p, and the total contact pressure p_z can be decomposed as $p^{(i)}{}_z = p^{(i)} + q^{(i)}$. If the two contact surfaces move only in the xz plane, then they can be decomposed in the x and z directions as $p_1^{(i)} = p_{x1}^{(i)}x + p_{z1}^{(i)}z$, $p_2^{(i)} = -p_{x2}^{(i)}x - p_{z2}^{(i)}z$ and $q_1^{(i)} = q_{x1}^{(i)}x - q_{z1}^{(i)}z$, $q_2^{(i)} = -q_{x2}^{(i)}x + q_{z2}^{(i)}z$, where, $p_1^{(i)}$ and $p_2^{(i)}$, $q_1^{(i)}$ and $q_2^{(i)}$ are projected with equal magnitude and opposite direction in the corresponding directions. The relationship between the slope at each contact point and the contact pressure at that point is as follows: $\partial z1/\partial x1 = -\partial z2/\partial x2 = q_{x1}^{(i)}/q_{z1}^{(i)} = q_{x2}^{(i)}/q_{z2}^{(i)} = p_{z1}^{(i)}/p_{x1}^{(i)} = p_{z2}^{(i)}/p_{x2}^{(i)}$, combined with V_z over its spatial micro-contact area A_i (i = 1, 2, ..., n) to sum up separately as follows:

$$\sum_i \iint_{A_i} \left[\frac{\partial \delta_z^{(i)}}{\partial t} p_{x1}^{(i)} \right] da_i = V_x \sum_i \iint_{A_i} p_{z1}^{(i)} da_i - V_z \sum_i \iint_{A_i} p_{x1}^{(i)} da_i \quad (1)$$

$$\sum_i \iint_{A_i} \left[\frac{\partial \delta_z^{(i)}}{\partial t} q_{x1}^{(i)} \right] da_i = V_x \sum_i \iint_{A_i} q_{z1}^{(i)} da_i - V_z \sum_i \iint_{A_i} q_{x1}^{(i)} da_i \quad (2)$$

Integrating the sum over A_i for both sides of $V_z = \partial h/\partial t$ gives the true contact area

(A_r) of the two contact surfaces as,

$$V_z \sum_i \iiint_{A_i} \mathrm{d}a_i = V_x \sum_i \iiint_{A_i} \frac{\partial z_1}{\partial x_1} \mathrm{d}a_i - \sum_i \iiint_{A_i} \frac{\partial \delta_z^{(i)}}{\partial t} \mathrm{d}a_i \quad (3)$$

where A_0 is a constant, A_r is the true contact area, and E_0 is the rate of change in time of the deformation in the z-direction, respectively:

$$A_0 = \sum_i \iiint_{A_i} \frac{\partial z_1}{\partial x_1} \mathrm{d}a_i \quad A_r = \sum_i \iiint_{A_i} \mathrm{d}a_i \quad E_0 = \sum_i \iiint_{A_i} \frac{\partial \delta_z^{(i)}}{\partial t} \mathrm{d}a_i \quad (4)$$

Suppose that the *z* direction component and the *x* direction component of molecular interaction force on the whole contacting surface are R_{z1} and R_{z2}, respectively. The *z* direction component and the *x* direction component of mechanical deformation resistance on the whole contacting surface are T_{z1} and T_{z2}, respectively. Here set the left side of Eqs. 1 and 2 as $W(1)$ and $W(2)$ respectively and descend into Eq. 3 to get $V_z[R_{x1}/W(1)-A_r/E_0]+V_x[A_0/E_0-R_{z1}/W(1)]=0$, $V_z[T_{z1}/W(2)-A_r/E_0]+V_x[A_0/E_0-T_{x1}/W(2)]=0$. This yields $R_{z1}=(A_0/A_r)R_{x1}=cR_{x1}$,and $T_{x1}=(A_0/A_r)T_{x1}=cT_{x1}$ (let $c=A_0/A_r$). Let the shear strength of the mould hole material be τ and A_{rp} be the plastic contact area, then we have $A_{rp}=R_{x1}/\tau$. If the normal load between the inner surface of the mould hole and the contact surface of the moulded particles is F_N, then we know that $F_N=R_{z1}+T_{z1}$, so the friction force $F=R_{x1}+T_{x1}=cF_N+(1-c^2)\tau A_{rp}$ is generated between the inner surface of the mould hole and the moulded particles.

The rough surface self-affine fractal features, therefore based on the rough surface fractal characterization and Hertz theory (Liu *et al*. 2020), then get the equation as follows,

$$A_{rp} = \left(\frac{D}{2-D}\right)^{(2-D)/2} \psi^{(2-D)^2/4} A_r^{D/2} G^2 \left(\frac{\pi E^2}{225\sigma_y^2}\right)^{(2-D)/2(D-1)} \quad (5)$$

where *D* is the fractal dimension of the surface profile; Ψ is the coefficient; a_c is the critical area at the micro-contact point when plastic change occurs (m^2); *G* is the fractal dimensional characteristic coefficient (m); σ_y is the yield strength of the material (Pa); and *E* is the composite modulus of elasticity of the friction substrate (Pa).

EXPERIMENTAL

Materials

Two biomass materials *Caragana korshinskii* twig (known as desert caragana) and maize stover (without the cobs) were selected in summer and autumn in the sandy areas of western Inner Mongolia) to prepare the caragana material molding pellets (Fig. 1). The granularity of the raw material pellets ranged from 1 to 4 mm and the average value of moisture content was 13%.

Instruments

The main test equipment included a JB-8C type precision roughness meter (YDYQ Precision Instrument Co., Ltd., Guangzhou, China); DHS-10A Rapid Moisture Tester (Lichen-BX Instrument Technology Co., Ltd., Shanghai, China); standard test sieve with 3-mm sieve pore as per GB/T 6003.1-2012 "Test Sieve Technical Requirements and Inspection" (Xinxiang Xiyang Yang Screening Machinery Manufacturing Co., Ltd., Xinxiang, China); JAEIHAENE type electronic scale (accuracy 0.01 g, Ruian Deli Business Electronics Co., Ltd., Ruian, China); Model LX-D Shore hardness tester (Leqing

Eidelberg Instruments Co., Ltd., Leqing, China); 100 mL measuring cylinder (accuracy 1 mL, Tianchang Tianhu Analytical Instruments Co., Ltd., Tianchang, China); and vernier calipers (Wuxi Xigong Gauge Co., Ltd., Wuxi, China).

Parameters Determination

Six types of molding pellets were compressed using a ring molding machine with a molding die-hole diameter d_0 of 8 mm. These 6 kinds of pellets were compressed from a mixture of 3 ratios of maize stover and caragana in summer and autumn. A total of 480 of them were taken for the study, and their diameter d, density ρ, hardness, and water content were measured. A roughness meter was used to measure the roughness morphology of its circumference surface and extract data. Then the parameters were compared for analysis of factors affecting the surface roughness morphology of the molding particles.

RESULTS AND DISCUSSION

Surface Parameters of Caragana and Stover Mixed Molding Pellets

Eighty samples of each of the six types of caragana branches mixed with stover in different proportions with a diameter of Φ8 mm were randomly selected. The actual diameter d, mass m, and hardness of the samples were measured. The average density value ρ of the sample was calculated from the volume and the mass m, and the volume could be obtained from the diameter d and the length. The surface roughness of the circumference of the molding particles was measured using a roughness meter, and its data were extracted. Then, according to the actual diameter d value, the 80 samples were divided into 8 groups and the average value of each parameter was taken. The results are shown in Tables 1 and 2. R_a indicates the arithmetic mean deviation of the assessed profile, R_c indicates the profile support length rate, R_z indicates the ten-point average height of microscopic unevenness, R_{sm} indicates the average width of the profile, and R_{pc} denotes the number of wave crests, M_{r2} indicates the maximum material rate of the roughness center profile, R_{ku} indicates roughness kurtosis, and R_{sk} indicates roughness skew.

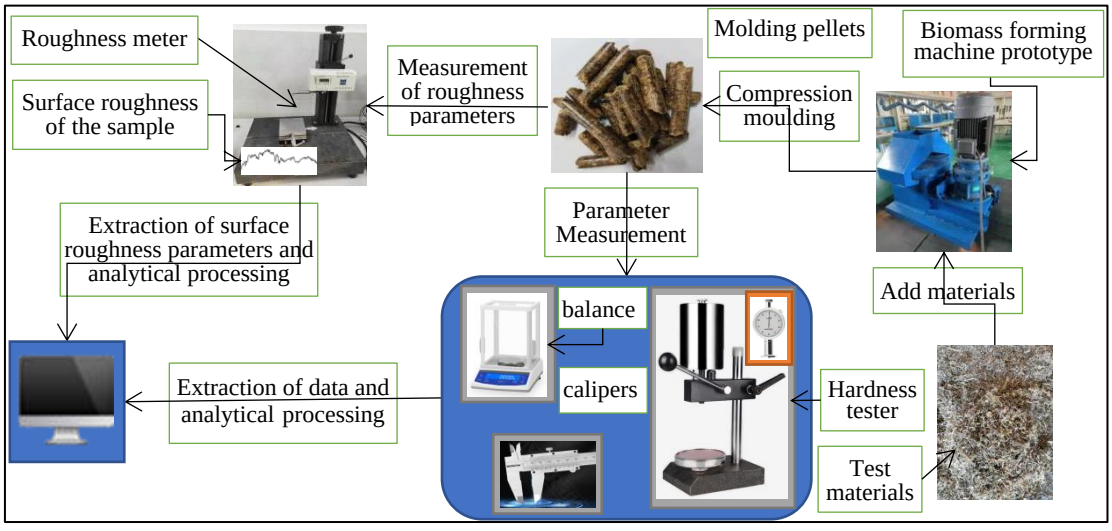

Fig. 2. Molding particle test rig as well as density, hardness, and circumferential rough surface topography measurement system

Table 1. Mean Values for Each Parameter of the Circumferential Surface of Caragana and Stover Mixed Molding Pellet in Summer

Material	Sample Group	*d* (mm)	*ρ* (g×cm^{-3})	Hardness (HD)	R_a (μm)	R_c (μm)	R_z (μm)	R_{sm} (mm)	R_{pc} pks×mm^{-1}	M_{r2} (%)	R_{sk}	R_{ku} (μm)
caragana+0%stover	1	8.07	1.214	64.9	1.250	0.625	11.276	0.190	27.5	89.3	-1.565	8.621
	2	8.09	1.191	64.1	1.425	0.713	8.006	0.222	27.5	86	-0.349	2.843
	3	8.15	1.188	62.7	1.684	0.842	10.763	0.286	30	82.1	-0.946	5.076
	4	8.22	1.171	61.1	2.017	1.008	13.601	0.364	20	90.5	-0.898	4.366
	5	8.31	1.157	58.4	2.214	1.107	14.732	0.235	25	87.1	-0.934	4.247
	6	8.43	1.133	56.3	2.603	1.302	18.280	0.286	22.5	84.9	-1.360	5.945
	7	8.51	1.077	55.1	3.057	1.528	20.994	0.267	25	83.8	-0.579	5.411
	8	8.57	1.026	53.5	3.348	1.674	25.366	0.286	30.0	82.5	-1.420	6.340
caragana+8%stover	1	8.11	1.189	64.1	1.353	0.676	9.205	0.235	30	90.6	-0.884	5.693
	2	8.15	1.171	63.7	1.704	0.852	9.540	0.308	22.5	81.3	-1.024	3.868
	3	8.24	1.161	62.3	1.975	0.988	12.249	0.211	25	87.2	-0.858	3.585
	4	8.29	1.159	61.4	2.057	1.028	13.381	0.308	25	84.9	-0.707	4.455
	5	8.38	1.141	57.7	2.486	1.243	18.980	0.333	20	81.2	-1.194	7.000
	6	8.44	1.127	55.2	2.838	1.419	21.305	0.444	22.5	83.7	-1.770	6.995
	7	8.53	1.071	53.5	3.213	1.607	21.660	0.235	30.0	84.8	-0.382	4.260
	8	8.66	1.011	51.4	3.480	1.740	19.603	0.364	20.0	85.7	-0.102	4.027
caragana+15%stover	1	8.13	1.185	63.5	1.420	0.710	7.680	0.286	30.0	80.8	-0.690	3.055
	2	8.18	1.177	62.2	1.852	0.926	11.228	0.333	20	83	-0.362	3.408
	3	8.23	1.155	60.3	2.324	1.162	12.225	0.308	20	79.8	-1.037	3.374
	4	8.35	1.130	58.8	2.501	1.250	15.778	0.333	25	79	-1.389	6.705
	5	8.42	1.121	57.1	2.684	1.342	13.366	0.286	32.5	80.2	-0.410	4.069
	6	8.49	1.114	53.7	3.302	1.651	23.909	0.308	22.5	82.1	-1.591	6.408
	7	8.56	1.008	51.3	3.485	1.742	19.886	0.222	30	85.6	0.152	3.690
	8	8.64	1.003	49.5	4.037	2.018	30.985	0.400	17.5	83.1	-1.261	5.826

Table 2. Mean Values for Each Parameter of the Circumferential Surface of Caragana and Stover Mixed Molding Pellet in Autumn

Material	Sample Group	d (mm)	ρ (g×cm^{-3})	Hardness (HD)	R_a (μm)	R_c (μm)	R_z (μm)	R_{sm} (mm)	R_{pc} (pks×mm^{-1})	M_{r2} (%)	R_{sk}	R_{ku} (μm)
caragana+ 0%stover	1	8.01	1.301	70.2	0.956	0.478	5.916	0.250	30	93.2	-0.273	3.350
	2	8.09	1.295	68.7	1.486	0.743	11.362	0.190	37.5	88	-1.115	6.606
	3	8.16	1.241	67.9	1.604	0.802	9.478	0.267	35	88	-0.495	3.777
	4	8.23	1.225	65.1	2.107	1.054	16.454	0.444	22.5	86.3	-1.080	7.575
	5	8.32	1.207	63.8	2.238	1.119	14.833	0.286	22.5	85.9	-0.280	4.760
	6	8.41	1.194	62.1	2.557	1.278	15.351	0.444	15	87.7	-0.333	5.650
	7	8.62	1.201	60.4	2.697	1.349	16.861	0.364	22.5	84.1	-0.905	4.738
	8	8.75	1.176	55.7	3.164	1.582	19.359	0.286	25	86.2	-1.035	5.586
caragana+ 8%stover	1	8.07	1.292	69.1	1.099	0.549	4.871	0.333	25	88.2	0.312	2.369
	2	8.15	1.281	66.9	1.531	0.765	7.244	0.235	27.5	92.2	-0.240	2.733
	3	8.21	1.270	64.1	1.765	0.882	15.068	0.444	12.5	88.6	-1.673	8.526
	4	8.33	1.255	62.8	2.093	1.046	15.174	0.400	15	87.3	-0.703	5.867
	5	8.41	1.234	58.9	2.272	1.136	15.485	0.286	20	87.8	-0.736	4.884
	6	8.47	1.211	57.3	2.569	1.284	12.618	0.308	30	85.8	-0.278	2.882
	7	8.57	1.204	56.2	2.766	1.383	16.621	0.308	20	86.1	0.043	3.259
	8	8.62	1.173	56.7	3.214	1.607	23.635	0.400	20	83.3	-0.494	4.334
caragana+ 15%stover	1	8.13	1.274	67.3	1.361	0.680	9.181	0.222	40	85.2	-0.674	4.636
	2	8.28	1.263	65.8	1.406	0.703	7.680	0.286	25	86.6	-0.048	2.730
	3	8.39	1.255	64.4	1.693	0.847	12.100	0.190	30	89.6	-1.124	5.767
	4	8.44	1.243	62.4	2.001	1.000	10.490	0.267	17.5	87.7	0.020	4.177
	5	8.53	1.231	61.3	2.139	1.069	15.447	0.211	35	83.4	-1.273	5.557
	6	8.65	1.237	59.5	2.466	1.233	17.719	0.267	27.5	82.4	-0.966	5.455
	7	8.75	1.217	57.6	2.934	1.467	7.542	0.222	25	86.5	-0.879	4.056
	8	8.77	1.201	56.3	3.372	1.686	23.726	0.333	20	82.8	-1.606	6.014

Relationship between the Diameter of the Molding Particles and their Density, Hardness, and Rough Surface Parameters

Figure 3 shows the relationship between pellet diameter *d* and density *ρ* for caragana mixed with maize stover in summer and autumn. Figure 4 shows the relationship between diameter *d* and hardness (HD) for caragana mixed with maize stover in summer and autumn. The density *ρ* and hardness HD of the six molded pellets tend to decrease as diameter *d* of the molded pellets increases. These changes were attributed mainly to an increase in diameter d_0 caused by the frictional wear of the material during the extrusion process of the mould holes in the molding machine. The length to diameter ratio h/d_0 of the molded holes decreased, which in turn made the density *ρ* and hardness HD of the molded pellets decrease. It can also be seen from the graph that the density *ρ* and hardness HD of the caragana mixed with stover molding pellets was somewhat greater in autumn than in summer overall, mainly because the fact that autumn lemons have thicker rhizome and higher biophysical properties (modulus of elasticity, shear modulus) than summer ones, which could also indicate that the summer caragana is suitable for feed and the autumn caragana could be considered for development as a biomass fuel.

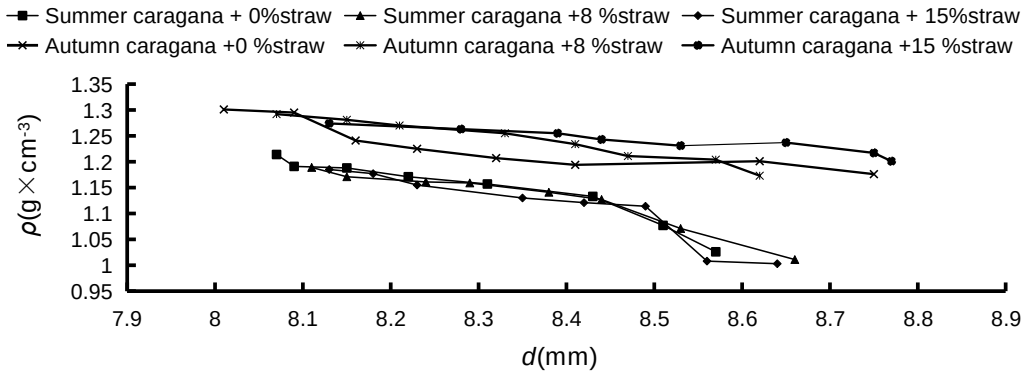

Fig. 3. Relation between diameter *d* and density *ρ*

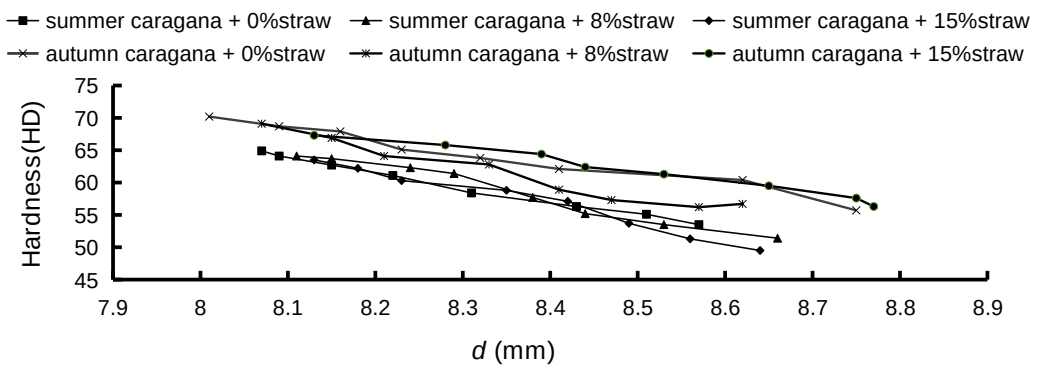

Fig. 4. Relation between diameter *d* and hardness HD

Figure 5 shows the relationship between the diameter *d* of the caragana and stover hybrid forming pellets and the arithmetic mean roughness parameters R_a and R_c. Figure 6 shows the relationship between the diameter *d* and the arithmetic mean roughness parameters R_z and R_{pc}. The arithmetic mean roughness parameters correspond to the circumferential surface.

The values of the roughness parameters R_a, R_c, and R_z on the circumferential surfaces of the six molded particles all tend to increase as their diameter *d* increases, while

the values of the roughness parameter R_{pc} tend to decrease as the diameter d increases. This is mainly because the decrease in density ρ of the formed particles leads to a decrease in the dense state of the particles and the circumferential surface shape is no longer smooth, resulting in higher values of the roughness parameters R_a, R_c and R_z; At the same time, due to the increased wear on the inner surface of the forming die hole, the crests on the inner surface are partially worn away and the roughness crest number R_{pc} decreases, which in turn leads to a decrease in the R_{pc} of the forming particles. It can also be seen from the graph that the surface roughness parameters R_a and R_c of the circumference of mixed forming pellets of autumn caragana were slightly smaller in autumn than in summer. This was mainly because caragana has a higher density ρ of compression molded pellets in autumn compared to summer, which also indicates that the summer caragana is more suitable for fodder and the autumn caragana can be used as biomass forming fuel (with relatively high coal-like characteristics).

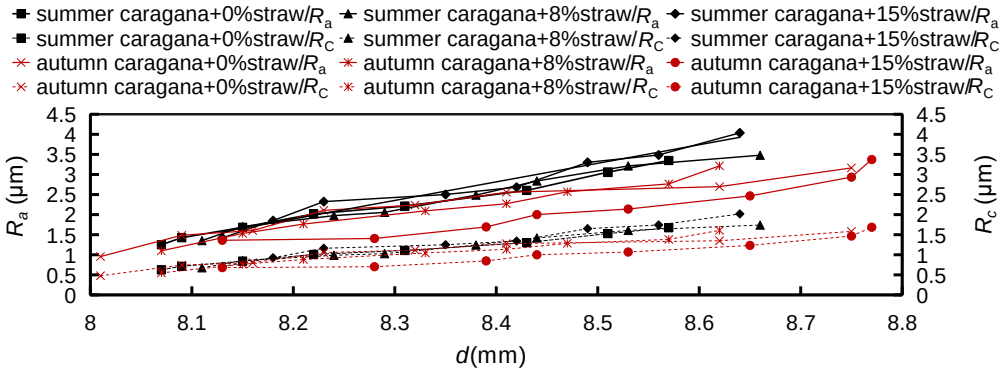

Fig. 5. Relation between diameter d and surface roughness parameters R_a, R_c

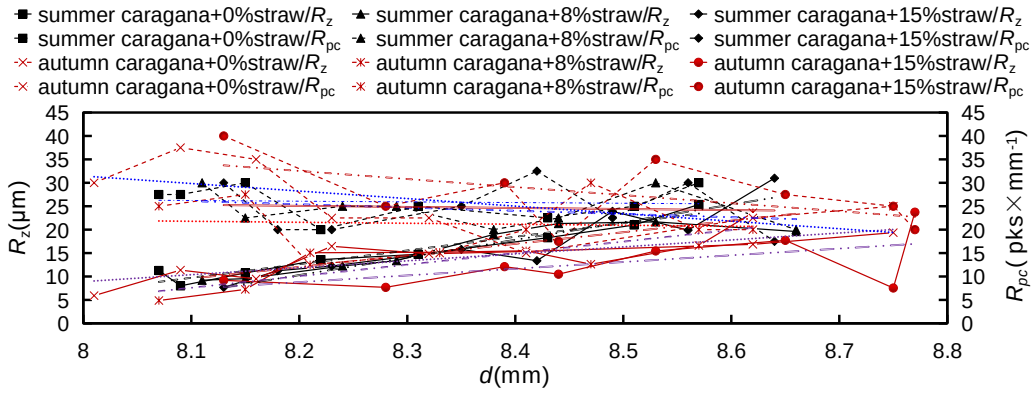

Fig. 6. Relation between diameter d and surface roughness parameters R_z, R_{pc}

Figure 7 shows the relationship between the diameter d of the caragana and stover hybrid forming pellets, the maximum material rate M_{r2} of the roughness center profile, and the surface roughness parameter R_{sm}. The maximum material rate M_{r2} of the roughness centre profile of the circumferential surface of the six types of molded particles basically remains around 86% as the diameter d of the molded particles increases. Moreover, it is generally in the range of 80% to 90%, with no obvious upward or downward trend. The maximum material rate M_{r2} value of the central profile of the roughness is a key parameter for the establishment of the mechanical model of the contact between the forming die hole and the forming particles (Falconer 1989; Huang 2020), and the constant parameter M_{r2} is beneficial for the establishment of the fractal contact model between the forming die hole

and the forming particles and the prediction model of frictional wear (Shi *et al*. 2020; An *et al*. 2020). In addition, the average width R_{sm} values of the roughness profile elements on the circumferential surfaces of the six molded particles have a small upward trend with increasing molded particle diameter *d*. This is mainly due to the decrease in the number of roughness waves R_{pc}, which is in line with the roughness morphology characteristic mechanism.

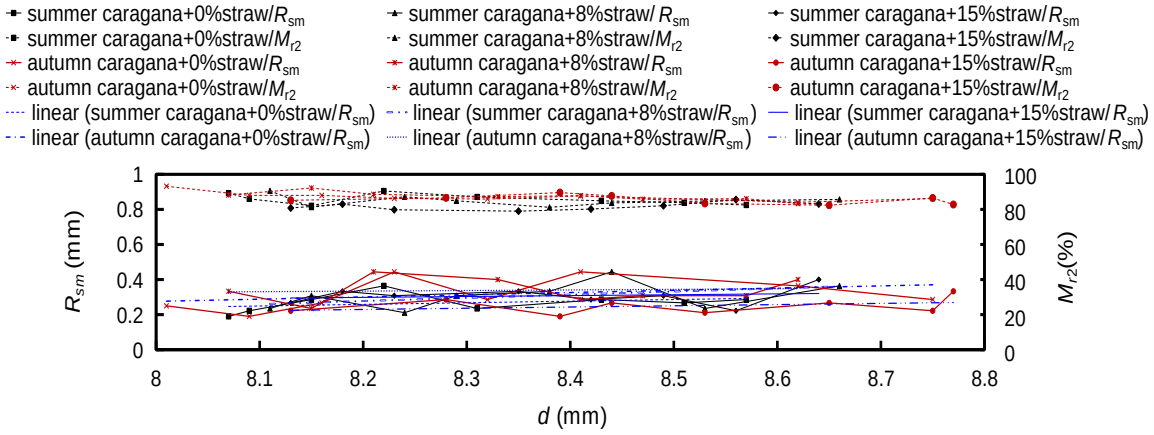

Fig. 7. Relation between diameter *d* and surface roughness parameters R_{sm}, M_{r2}

The Relationship between the Diameter of the Molding Particles and their Surface Roughness Morphology

Figure 8 shows the relationship between the diameter *d* of the six types of caragana and stover blended molding pellets and the shape sharpness R_{ku} (roughness kurtosis) of the roughness profile height amplitude curve relative to the average line. Figure 9 exhibits the relationship between diameter *d* and the asymmetric skew R_{sk} (roughness skew) of the profile height amplitude curve relative to the average line.

It can be seen (Figs. 8, 9) that the kurtosis R_{ku} and the skew R_{sk} of the roughness of the molded particles showed no obvious rising or falling trend as the diameter *d* of the molded particles increased. Furthermore, $R_{ku}>3$ (the overall trend is in the range of 3 to 6), which indicates that the surface profile height amplitude distribution curve of the molded particles had a spiky form surface and a high kurtosis value. There was also $R_{sk}<0$ (the overall trend is in the -0.5 to -1 range) (An *et al.* 2020; Huang *et al.* 2020; Xiao *et al.* 2020; Shi *et al.* 2020; Zhang *et al.* 2020), which indicates that the surface of the caragana particles had an asymmetric contour profile and exhibited a negative skew direction, a low number of peak tips, and had good surface bearing properties.

The graphs also show that the surface of the caragana and stover mixed molding pellets was slightly closer to 0 in terms of roughness skew R_{sk} and slightly closer to 3 in terms of roughness kurtosis R_{ku} in the autumn compared to the summer. This indicates that the surface morphology of the autumn caragana molding pellets was closer to the excellent kurtosis values of the arbitrary surface, the asymmetric surface profile, and the low negative skew. This was mainly attributed to the higher biophysical properties (modulus of elasticity, modulus of shear) of the autumn caragana compared to the summer caragana, so that the surface shape after compression is close to a symmetrical surface profile pattern.

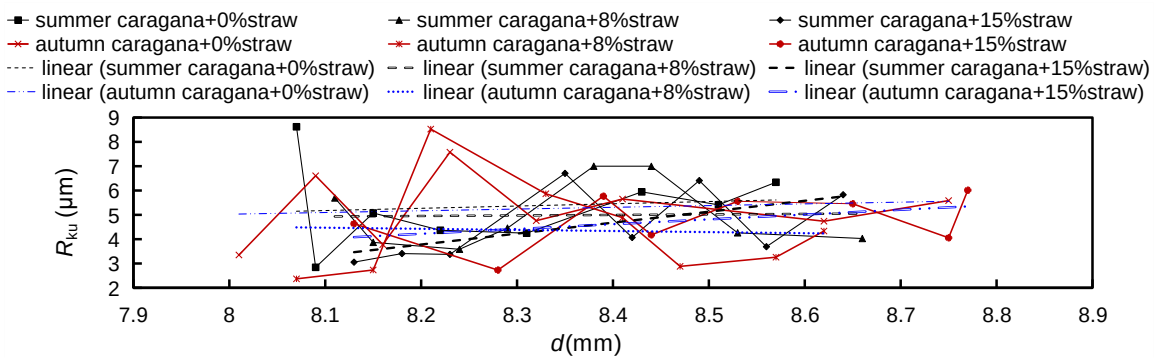

Fig. 8. Relationship between diameter *d* and roughness kurtosis R_{ku}

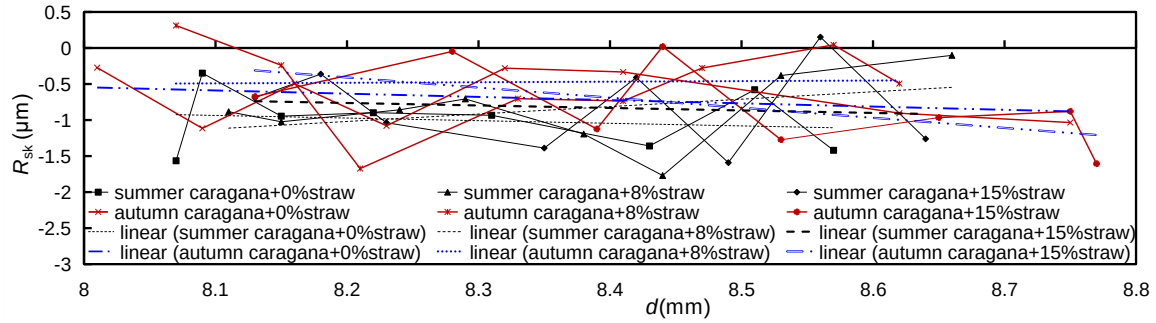

Fig. 9. Relationship between diameter *d* and roughness skew R_{sk}

CONCLUSIONS

1. The forming die hole of the biomass ring molding machine generates frictional wear during contact with the desert caragana (*Caragana korshinskii*) and maize stover mixture forming pellets, resulting in an increase in the forming die hole diameter d_0 and a corresponding increase in the forming pellet diameter *d*. The degree of frictional wear of the mold hole is related to the mixture of caragana and stover, the material of the mold hole, and the time of frictional wear.
2. The density ρ and hardness HD of the formed pellets tend to decrease with increasing diameter *d*. This is because an increase in the diameter d_0 of the mold hole of the forming machine reduces the length-to-diameter ratio of the mold hole, which in turn makes the density of the formed pellets smaller and their quality lower. The ρ and HD of these caraganas are higher in autumn than in summer due to their higher physical characteristics in autumn, which makes summer caragana suitable for fodder, and autumn caragana can be developed as biomass fuel.
3. The values of the roughness parameters R_a, R_c,and R_z of the molded particles tend to increase with their diameter *d*. This is because an increase in the diameter d_0 of the mold hole causes the density of the molded particles to decrease and the surface of the molded particles to become rougher. The maximum material rate M_{r2} value for the central profile of the roughness of the circumferential surface stays roughly around 86% as the diameter *d* of the molded particles increases.
4. Molded pellets with increasing diameter *d* have a surface roughness kurtosis $R_{ku}>3$ and roughness skew $R_{sk}<0$, indicating that the surface morphology of molded pellets is a spiky surface, a negatively skewed surface of asymmetrical profile with a small number

of spikes and better surface characteristics. The surface morphology of the autumn caragana molding pellets is closer to the excellent kurtosis values of the arbitrary surface, the asymmetric surface profile, and the low negative skew. This is mainly due to the higher biophysical properties of the autumn caragana compared to the summer caragana, so that the surface shape after compression is close to a symmetrical surface profile pattern.

ACKNOWLEDGMENTS

The authors are grateful to Wenbin Guo from Inner Mongolia Agricultural University, Hohhot, China, for help with laboratory analysis work. The authors are also grateful for the support of the National Natural Science Foundation of China (NSFC) Project (51766016; 31960365; 32060414).

REFERENCES CITED

An, Q., Suo, S. F., Lin, F. Y., Bai, Y. Z., Geng, H. X., and Shi, J. W. (2020). "Microscopic contact model for surface grinding of rough surfaces," *Journal of Mechanical Engineering* 56(07), 240-248. DOI: 10.3901/JME.2020.07.240

De, X. H., Zhang, J. C., Yang, Y., Du, J. Q., Guo, W. B., and Li, Z. (2021). "Fractal prediction of frictional force against the interior surface of forming channel coupled with temperature in a ring die pellet machine," *BioResources* 16(3), 4780-4797. DOI: 10.15376/biores.16.3.4780-4797

De, X. H., Yu, G. S., and Zhai, X. M. (2014). "Numerical analysis of frictional heat in plunger ring moulds," *Chinese Journal of Non-Ferrous Metals* 24(06), 1578-1584. DOI: 10.19476/j.ysxb.1004.0609.2014.06.024

Duan, J., and Chen, S. R. (2017). "Preferential selection and testing of ring die hole type for ring die straw briquetting machine," *Agricultural Mechanization Research* (02), 122-128. DOI: 10.13427/j.cnki.njyi.2017.02.045

Falconer, K. (1989). *Fractal Geometry: Mathematical Foundation Sand Applications*, John Wiley, New York, NY.

Ge, S. R., and Zhu, H. (2005). *Fractal of Tribology*, 1st Ed., Machinery Industry Press, Beijing, China.

Huang, S. Z., Liu, J., and Shen, H. M. (2020). "Numerical study on the effect of initial roughness on tangential micro-motion behavior," *Journal of Sichuan Light Chemical University (Natural Science Edition)* 33(03), 13-18. DOI: 10.11863/j.suse.2020.03.03

Huang, Y. K. (2020). *Study on Contact Model of Rough Surface with Real Topography*, North University of China, Taiyuan, China. DOI: 10.27470/d.cnki.ghbgc.2020.000216

Jiang, Y. S., Wang, G. M., Wu, Y., Chen, F. S., and Ji, Z. (2020). "Advances in biomass-based coal technology in China," *Biochemicals* 6(06), 164-166+172. DOI: 10.3969/j.issn.2096-0387.2020.06.045

Jiao, Y. H. (2020). "Exploring the development prospect of China's biomass energy industry," *Journal of Economic Research* (25), 44-45. DOI: 10.3969/j.issn.1673-291X.2020.25.018

Liu, K. A., Xu, Y. Q., Wu, Z. H., and Xiao, L. (2020a). "Analysis of the evolutionary behavior of fractal surface plus and minus normal contact stiffness," *Journal of Northwestern Polytechnical University* 38(06), 1188-1197. DOI: 10.3969/j.issn.1000-2758.2020.06.007

Liu, Y., Xia, T., Chen, Z.Y., and Yan, G. H. (2020b). "Proposed and development of statistical contact models for rough surfaces," *Journal of Tribology* 40(03), 395-406. DOI: 10.16078/j.tribology.2019191

Mao, X. (2021). "Promoting clean heating in rural areas under the background of population hollowing: Challenges and countermeasures," *China and Foreign Energy* 26(04), 14-20.

Nieslony, P., Krolczyk, G. M., Wojciechowski, S., Chudy, R., Zak, K., and Maruda, R.W. (2018). "Surface quality and topographic inspection of variable compliance part after precise turning," *Applied Surface Science* 434(15), 91-101. DOI: 10.1016/j.apsusc.2017.10.158

Ning, T. Z., Ma, A. J., Yu, Y., and Chen, Z. J. (2016). "Analysis of the problems and countermeasures of biomass ring die pellet forming," *China Journal of Agricultural Chemistry* 37(01), 272-276. DOI: 10.13733/j.jcam.issn.2095-5553.2016.01.061

Qiu, P., Li, X. X., Zhao, T.S., and Liu, S. S. (2020). "Analysis and test of wear resistance mechanism of straw briquetting machine roll mouth type ring die," *Journal of Agricultural Machinery* 37(01), 272-276. DOI: 10.6041/j.issn.1000-1298.2016.03.016

Schweinhart, B. (2020). "Fractal dimension and the persistent homology of random geometric complexes," *Advances in Mathematics* 372, article 107291. DOI: 10.48550/arXiv.1808.02196

Shi, X., Wang, W., Liu, K., Chen, R., Yang, L., and Feng, S. Y. (2020). "Construction of a finite element model for microscopic random rough surface contact and contact analysis," *Lubrication and Seals* 45(05), 25-29. DOI: CNKI:SUN:RHMF.0.2020-05-007

Song, Y., Liu, B. G., Ren, D. R., Yu, M. Y., and Huang, R. (2021). "A method for constructing stochastic rough joint models based on fractal theory," *Journal of Rock Mechanics and Engineering* 40(01), 101-112. DOI: 10.13722/j.cnki.jrme.2020.0487

Wang, J., Wu, Y. Q., Li, X. J., and Zuo, Y. F. (2021). "Current status of research on resource utilization of rice/wheat straw," *Forest Industry* 58(01), 1-5. DOI: 10.19531/j.issn1001-5299.202101001

Xiao, Y. Y., Wu, L. L., Luo, J., and Zhou, L. H. (2020). "Mechanical response of thin hard coatings under indentation considering rough surface and residual stress," *Diamond & Related Materials* 108, article 107991. DOI: 10.1016/j.diamond.2020.107991

Yu, L. (2021). "Current status and future trends of biomass combustion technology development," *Applied Energy Technology* (04), 16-18. DOI: 10.3969/j.issn.1009-3230.2021.04.005

Zhang, J. C., De, X. H., Li, Z., Guo, W. B., and Yu, L. K. (2020a). "Current status of research on biomass curing and molding mechanism and equipment," *Forest Industry* 57(12), 45-49. DOI: 10.19531/j.issn1001-5299.202012009

Zhang, Y. Q., Lu, H., Zhang, X. B., He, L., Wei, F., Liu, B., and Guo, Z. X. (2020b). "A normal contact stiffness model of machined joint surfaces considering elastic, elasto-plastic and plastic factors," *Journal of Engineering Tribology* 234(07), 1007-1016. DOI: 10.1177/1350650119867801

Zhang, Y. W., Yu, G. S., Ji, Y., Hao, Q., Liang, Y., and Wang, J. M. (2021). "Design of forming mould for plunger type press roll biomass forming machine," *Journal of Northwest Agriculture and Forestry University of Science and Technology (Natural Science Edition)* 49(04), 142-154. DOI: 10.13207/j.cnki.jnwafu.2021.04.016

Article submitted: January 8, 2023; Peer review completed: February 18, 2023; Revised version received and accepted: February 21, 2023; Published: March 2, 2023.
DOI: 10.15376/biores.18.2.3019-3032